Evaluation of geometrically nonlinear terms in the large-deflection and post-buckling analysis of isotropic rectangular plates

Alfonso Pagani[a,*], Ehsan Daneshkhah[a,†], Xiangyang Xu[a,‡], Erasmo Carrera[a,§],

[a]Mul^2 Group, Department of Mechanical and Aerospace Engineering,
Politecnico di Torino, 10129 Torino, Italy;

Abstract:

The nonlinear mechanical response of highly flexible plates and shells has always been of primary importance due to widespread applications of these structural elements in many advanced engineering fields. In this study, the Carrera Unified Formulation (CUF) is used in a total Lagrangian framework to analyze the large-deflection and post-buckling behavior of isotropic rectangular plates based on different nonlinear strain assumptions. The scalable nature of CUF provides us with the ability to tune the structural theory approximation order and the strain-displacement assumptions opportunely. In this work, the Newton- Raphson linearization scheme with a path-following constraint is used in the framework of 2-D CUF to solve the geometrically nonlinear problems to draw important conclusions about the consistency of many assumptions made in the literature on the kinematics of highly flexible plates. In this regard, the effectiveness of the well-known von Kármán theory for nonlinear deformations of plates is investigated with different modifications such as the thickness stretching and shear deformations due to transverse deflection. The post-buckling curves and the related stress distributions for each case are presented and discussed. According to the results, the full Green-Lagrange nonlinear model could predict the nonlinear behavior of plates efficiently and accurately, whereas other approximations produce considerable inaccuracies in the case of thick plates subjected to large rotations and deflections.

Keywords: Carrera Unified Formulation; Geometrical nonlinear plates; Green-Lagrange strains, Nonlinear geometric relations.

---

1 Introduction

Highly flexible plate structures are used extensively in different engineering applications. Many applications of plates can be found in the engineering; for instance, the use of very thin circular plates in computer hard disk drives, rectangular and trapezoidal plates in the wing skin, cantilever rectangular plates in nano-resonators for drug detection, and clamped circular thin nano-plates of graphene in nano-devices for pressure measurement [1]. Plates are initially flat structures having two dimensions much larger than the third one and can sustain extension, compression, in-plane shear, bending, twisting, and transverse shear loads [2]. Nonlinearity occurs in mathematical formulation of most physical problems. If certain quantities of the formulation are small, the problem may be considered linear. Two common sources of nonlinearity are geometry and material. The geometric nonlinearities arise purely from geometric consideration and nonlinear strain-displacement relations. On the other hand, the material nonlinearities arise due to the nonlinear constitutive behavior of

*Assistant Professor. E-mail: alfonso.pagani@polito.it
†Ph.D. student. E-mail: ehsan.daneshkhah@polito.it
‡Research fellow. Email: xuxiangyang@yahoo.com
§Full Professor. E-mail: erasmo.carrera@polito.it

the material of the system [3]. Due to the necessity of a safe and reliable design, the effects of these nonlinearities in the mechanical responses of plates have always been of fundamental importance.

Many studies have been carried out with the focus on the large deflections of plates [4, 5, 6, 7]. Levy [8, 9] presented theoretical analysis for the large deflections of plates. Rushton [10] investigated the large deflection of variable-thickness plates. Turvey and Osman [11] conducted a study on the large deflection of Mindlin plates and introduced the relevant governing equations using the Dynamic Relaxation method. Alijani and Amabili [12] introduced a numerical solution for nonlinear static bending and vibration of plates to predict the correct thickness stretching. The same authors carried out an analysis on functionally graded rectangular plates to investigate the effect of thickness deformation [13]. Wu et al. [14] studied the large deflection and post-buckling of thin and moderately thick plates by using Carrera Unified Formulation (CUF) and the Newton–Raphson linearization scheme combined with a path-following method. They presented the Fundamental Nucleus (FN) of secant and tangent stiffness matrices for the plates and investigated the effect of different boundary conditions on the large deflection analysis of plates.

Furthermore, some researchers focused on the large deflection of laminated plates [15, 16, 17]. Shukla and Nath [18] obtained analytical solutions for laminated-composite plates with geometrically nonlinear boundary value problems. Dash and Singh [19] presented a formulation for the nonlinear bending of laminated plates considering transverse shear and large rotations. Carrera and Kröplin [20] considered higher-order shear deformation theories for composite plates under large deflection and post-buckling. Coda et al. [21, 22] proposed FE formulation for nonlinear analysis of laminated plates and shells to obtain correct stress fields.

The post-buckling analysis of plates has been also studied by many researchers. Leissa [23] presented a report document on the buckling and post-buckling behavior of laminated composite plates and shells. Librescu and Chang [24] focused on the post-buckling in composite doubly-curved shallow panels and analyzed the imperfection sensitivity. Turvey and Marshall [25] worked on the buckling and post-buckling behavior of composite plates and prepared a comprehensive book on this. Pagani and Carrera [26] used the unified formulation in combination with the Newton–Raphson linearization method for geometrically nonlinear beams and formulated the Fundamental Nucleus of secant and tangent stiffness matrices of refined beam theories. The same authors conducted an analysis on the large-deflection and post-buckling of laminated composite beams [27]. Pagani et al. [28] investigated the effect of various geometrically nonlinear assumptions in the response of beam and thin-walled structures using a refined beam model in the domain of CUF with a total Lagrangian scenario.

The main aim of this article is to investigate the effect of different geometric nonlinear relations in the nonlinear analysis of plates using CUF. The use of CUF provides us with arbitrary expansions of any order along the thickness. In this research, Lagrange polynomials are considered as the functions for the expansion and different plate theories are considered with different orders of expansion through the thickness. The selection of nonlinear CUF, provides us with arbitrary expansion functions and the ability to consider different components of Green-Lagrange strain tensor. The Newton-Raphson linearization scheme with the path-following constraint is used in the 2-D CUF framework. This geometrically nonlinear model is validated with 1-D CUF for beam structures and other available literature. Strains approximation of von Kármán for plates is considered with different modifications and the equilibrium curves and relevant stress distributions are compared and discussed based on these nonlinear theories.

2 Preliminary considerations

If we consider a plate with the in-plane and through-the-thickness domains, respectively, in the $x-y$ plane and along the z axis, the displacement, the stress, and the strain vectors are as follows:

$$\mathbf{u}(x,y,z) = \{u_x \;\; u_y \;\; u_z\}^T$$

$$\boldsymbol{\sigma} = \{\sigma_{xx} \;\; \sigma_{yy} \;\; \sigma_{zz} \;\; \sigma_{xz} \;\; \sigma_{yz} \;\; \sigma_{xy}\}^T \tag{1}$$

$$\boldsymbol{\epsilon} = \{\varepsilon_{xx} \;\; \varepsilon_{yy} \;\; \varepsilon_{zz} \;\; \varepsilon_{xz} \;\; \varepsilon_{yz} \;\; \varepsilon_{xy}\}^T$$

Considering linear elastic homogeneous material, the constitutive relation is:

$$\boldsymbol{\sigma} = \mathbf{C}\boldsymbol{\epsilon}, \tag{2}$$

Interested readers are referred to text-books [30, 35] for more information about the explicit form of the material matrix C in the case of metallic structures, as in this article.

By using the Green-Lagrange strain tensor for the geometrical relations, the following equation could be considered between strain and displacement vectors.

$$\boldsymbol{\epsilon} = \boldsymbol{\epsilon}_l + \boldsymbol{\epsilon}_{nl} = (\mathbf{b}_l + \mathbf{b}_{nl})\mathbf{u}, \tag{3}$$

where the linear and nonlinear differential operators $\mathbf{b}_l$ and $\mathbf{b}_{nl}$ are defined as:

$$\mathbf{b}_l = \begin{bmatrix} \partial_x & 0 & 0 \\ 0 & \partial_y & 0 \\ 0 & 0 & \partial_z \\ \partial_z & 0 & \partial_x \\ 0 & \partial_z & \partial_y \\ \partial_y & \partial_x & 0 \end{bmatrix}, \qquad \mathbf{b}_{nl} = \begin{bmatrix} P_{11}\frac{1}{2}(\partial_x)^2 & P_{12}\frac{1}{2}(\partial_x)^2 & P_{13}\frac{1}{2}(\partial_x)^2 \\ P_{21}\frac{1}{2}(\partial_y)^2 & P_{22}\frac{1}{2}(\partial_y)^2 & P_{23}\frac{1}{2}(\partial_y)^2 \\ P_{31}\frac{1}{2}(\partial_z)^2 & P_{32}\frac{1}{2}(\partial_z)^2 & P_{33}\frac{1}{2}(\partial_z)^2 \\ P_{41}\partial_x\,\partial_z & P_{42}\partial_x\,\partial_z & P_{43}\partial_x\,\partial_z \\ P_{51}\partial_y\,\partial_z & P_{52}\partial_y\,\partial_z & P_{53}\partial_y\,\partial_z \\ P_{61}\partial_x\,\partial_y & P_{62}\partial_x\,\partial_y & P_{63}\partial_x\,\partial_y \end{bmatrix}, \tag{4}$$

in which $\partial_x = \partial(\cdot)/\partial x$, $\partial_y = \partial(\cdot)/\partial y$, $\partial_z = \partial(\cdot)/\partial z$, and P_{11} to P_{63} are the parameters used as coefficients of nonlinear differential operator matrix to tune the kinematics assumptions opportunely, see [28]. As will be discussed in the following sections of this article, the parameters of P_{ij} play an important role in the accuracy of the kinematic model of the problem and define the considered geometrically nonlinear theory.

For instance, in the case of well-known von Kármán theory [29], nonlinear geometric relations of the plate structures are:

$$\varepsilon_{xx_{nl}} = \tfrac{1}{2}(u_{z,x})^2$$

$$\varepsilon_{yy_{nl}} = \tfrac{1}{2}(u_{z,y})^2 \tag{5}$$

$$\varepsilon_{xy_{nl}} = u_{z,x}u_{z,y}$$

As shown in Fig. 1, von Kármán strains approximation neglects all the nonlinear quadratic terms of Eq. 4, except those which are related to the in-plane partial derivatives of the transverse displacement. Therefore, for the case of von Kármán nonlinear plate, all the parameters of Eq. 4 are zero except P_{13}, P_{23}, and P_{63}. The matrix of these parameters based on different nonlinear models is illustrated in Table 1. Based on Table 1, four modifications of the von Kármán nonlinear theory are considered in this paper with the notations of vK$_{+T}$, vK$_{+S}$, vK$_{+IN}$, and vK$_{+All}$. For completeness reasons, note that vK$_{+T}$, vK$_{+S}$, and vK$_{+IN}$ are referred to von Kármán nonlinear theory with the modification of thickness stretching, shear deformations due to transverse deflection, and in-plane components of the displacement. In addition, vK$_{+All}$ corresponds to von Kármán nonlinear theory with all previously mentioned modifications. As will be discussed in Section 4, the selection of the proper model for strain-displacement relations is vital for obtaining the reliable and accurate nonlinear response of the structure.

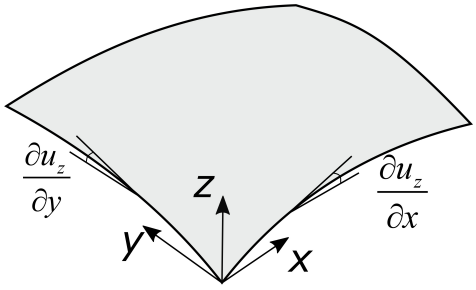

Figure 1: Main strain-displacement assumptions for the von Kármán nonlinear plate

Table 1: Geometrically nonlinear theories focused on in this research

Theory	Description	Notation	Theory	Description	Notation
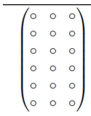	*Linear*	Lin	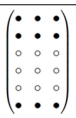	*von Kármán considering in-plane components of displacement*	vK_{+IN}
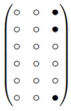	*von Kármán*	vK	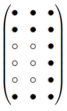	*von Kármán with all the mentioned considerations*	vK_{+All}
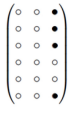	*von Kármán considering thickness stretching*	vK_{+T}	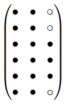	*Full Nonlinear without von Kármán terms*	FNL_{-vK}
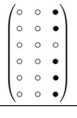	*von Kármán considering shear deformations due to transverse deflection*	vK_{+S}	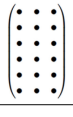	*Full Nonlinear*	FNL

3 Carrera Unified Formulation (CUF)

Based on the Carrera Unified Formulation (CUF) for 2-D structures [30], the three-dimensional displacement field is defined as a general expansion of primary unknowns as:

$$\mathbf{u}(x,y,z) = F_s(z)\mathbf{u}_s(x,y), \qquad s = 0,1,\cdots,N, \tag{6}$$

where F_s is the set of thickness functions and $\mathbf{u}_s$ is the generalized displacement vector. As it is clear from Eq. (6), the use of CUF provides us with arbitrary expansions of any order along the thickness. In this research, Lagrange polynomials are considered as the functions for the expansion (LE), which have been demonstrated to be very effective for several applications, including aerospace and civil structures [31, 32, 33, 34]. Note that in the case of LE, the unknown variables are pure displacements. Based on LE, different plate theories are considered by opportunely varying the expansion order. These models will be referred to as LDN (Langrange Displacement-based of order N). As an example, LD1, LD2, and LD3 are related to linear (two-node), quadratic (three-node), and cubic (four-node) Lagrange expansion functions.

By using the finite element method, the displacement vector $\mathbf{u}_s$ can be approximated based on the nodal parameters $\mathbf{q}_{sj}$ and shape functions N_j as:

$$\mathbf{u}_s(x,y) = N_j(x,y)\mathbf{q}_{sj}, \qquad j = 1,2,\ldots,p+1, \tag{7}$$

where N_j is the j-th shape function and p is related to the order of the shape functions. In this study, 2D nine node quadratic elements (Q9) are used for the shape function in the $x-y$ plane. More information abut Lagrange polynomials and shape functions can be found in [35].

3.1 Nonlinear governing equations

In this study, the Newton-Raphson method with a path-following constraint [36, 26, 27] is used in order to solve geometrically nonlinear plate problems. The principle of virtual work states that for arbitrary infinitesimal virtual displacement satisfying the prescribed geometrical constraints, the virtual variation of internal strain energy must be equal to the virtual variation of the work of external loadings [26]:

$$\delta L_{\text{int}} = \delta L_{\text{ext}} \tag{8}$$

The virtual variation of the internal strain energy in Eq. (8) can be calculated as:

$$\delta L_{\text{int}} = < \delta\boldsymbol{\epsilon}^{\mathrm{T}}\boldsymbol{\sigma} > \tag{9}$$

where $< (\cdot) >= \int_V (\cdot)\, dV$ and $V = \Omega \times h$ is the initial volume of the plate structure under the hypothesis of small deformations. δ represents the virtual variation operator. According to FEM approximation, CUF, the introduced constitutive equations, and geometric relations, it is proved that:

$$\begin{aligned}
\delta L_{\text{int}} &= \delta\mathbf{q}_{\tau i}^{\mathrm{T}} < \left(\mathbf{B}_l^{\tau i} + 2\,\mathbf{B}_{nl}^{\tau i}\right)^{\mathrm{T}} \mathbf{C} \left(\mathbf{B}_l^{sj} + \mathbf{B}_{nl}^{sj}\right) > \mathbf{q}_{sj} \\
&= \delta\mathbf{q}_{\tau i}^{\mathrm{T}} \mathbf{K}_0^{ij\tau s} \mathbf{q}_{sj} + \delta\mathbf{q}_{\tau i}^{\mathrm{T}} \mathbf{K}_{lnl}^{ij\tau s} \mathbf{q}_{sj} + \delta\mathbf{q}_{\tau i}^{T}\mathrm{T}\, \mathbf{K}_{nll}^{ij\tau s} \mathbf{q}_{sj} + \delta\mathbf{q}_{\tau i}^{\mathrm{T}} \mathbf{K}_{nlnl}^{ij\tau s} \mathbf{q}_{sj} \\
&= \delta\mathbf{q}_{\tau i}^{T} \mathbf{K}_S^{ij\tau s} \mathbf{q}_{sj}
\end{aligned} \tag{10}$$

where $\mathbf{K}_S^{ij\tau s} = \mathbf{K}_0^{ij\tau s} + \mathbf{K}_{lnl}^{ij\tau s} + \mathbf{K}_{nll}^{ij\tau s} + \mathbf{K}_{nlnl}^{ij\tau s}$ is the Fundamental Nucleus of the secant stiffness matrix.

Linearizing the virtual variation of the internal strain energy can yield the tangent stiffness matrix as:

$$\mathrm{d}(\delta L_{\text{int}}) = < \mathrm{d}(\delta\boldsymbol{\epsilon}^{\mathrm{T}}\boldsymbol{\sigma}) > = < \delta\boldsymbol{\epsilon}^{\mathrm{T}}\mathrm{d}\boldsymbol{\sigma} > + < \mathrm{d}(\delta\boldsymbol{\epsilon}^{\mathrm{T}})\boldsymbol{\sigma} > = \delta\mathbf{q}_{\tau i}^{\mathrm{T}} \mathbf{K}_T^{ij\tau s} \mathrm{d}\mathbf{q}_{sj} \tag{11}$$

where $\mathbf{K}_T^{ij\tau s} = \mathbf{K}_0^{ij\tau s} + \mathbf{K}_{T_1}^{ij\tau s} + \mathbf{K}_\sigma^{ij\tau s}$. The first term $< \delta\boldsymbol{\epsilon}^T \mathrm{d}\boldsymbol{\sigma} >$ in Eq. (11) requires the constitutive equation to linearized. Therefore:

$$\mathrm{d}\boldsymbol{\sigma} = \mathrm{d}(\mathbf{C}\boldsymbol{\epsilon}) = \mathbf{C}\mathrm{d}\boldsymbol{\epsilon} = \mathbf{C}(\mathbf{B}_l^{sj} + 2\,\mathbf{B}_{nl}^{sj})\mathrm{d}\mathbf{q}_{sj} \tag{12}$$

$$\begin{aligned} < \delta\boldsymbol{\epsilon}^{\mathrm{T}} \mathrm{d}\boldsymbol{\sigma} > &= \delta\mathbf{q}_{\tau i}^{\mathrm{T}} < (\mathbf{B}_l^{\tau i} + 2\,\mathbf{B}_{nl}^{\tau i})^{\mathrm{T}} \mathbf{C}\,(\mathbf{B}_l^{sj} + 2\,\mathbf{B}_{nl}^{sj}) > \mathrm{d}\mathbf{q}_{sj} \\ &= \delta\mathbf{q}_{\tau i}^{\mathrm{T}}\,\mathbf{K}_0^{ij\tau s}\mathrm{d}\mathbf{q}_{sj} + \delta\mathbf{q}_{\tau i}^{\mathrm{T}}\left(2\,\mathbf{K}_{lnl}^{ij\tau s}\right)\mathrm{d}\mathbf{q}_{sj} + \delta\mathbf{q}_{\tau i}^{\mathrm{T}}\,\mathbf{K}_{nll}^{ij\tau s}\mathrm{d}\mathbf{q}_{sj} + \delta\mathbf{q}_{\tau i}^{\mathrm{T}}\left(2\,\mathbf{K}_{nlnl}^{ij\tau s}\right)\mathrm{d}\mathbf{q}_{sj} \\ &= \delta\mathbf{q}_{\tau i}^{\mathrm{T}}\left(\mathbf{K}_0^{ij\tau s} + \mathbf{K}_{T_1}^{ij\tau s}\right)\mathrm{d}\mathbf{q}_{sj} \end{aligned} \tag{13}$$

where $\mathbf{K}_{T_1}^{ij\tau s} = 2\,\mathbf{K}_{lnl}^{ij\tau s} + \mathbf{K}_{nll}^{ij\tau s} + 2\,\mathbf{K}_{nlnl}^{ij\tau s}$ is the nonlinear contribution of the FN of the tangent stiffness matrix stemming from the linearization of the constitutive relation. For the term, $< \mathrm{d}(\delta\boldsymbol{\epsilon}^{\mathrm{T}})\boldsymbol{\sigma} >$, we have

$$\begin{aligned} < \mathrm{d}(\delta\boldsymbol{\epsilon}^{\mathrm{T}})\boldsymbol{\sigma} > &= < \begin{Bmatrix} \delta q_{u_{x_{\tau i}}} \mathrm{d}q_{u_{x_{sj}}} \\ \delta q_{u_{y_{\tau i}}} \mathrm{d}q_{u_{y_{sj}}} \\ \delta q_{u_{z_{\tau i}}} \mathrm{d}q_{u_{z_{sj}}} \end{Bmatrix}^{\mathrm{T}} (\mathbf{B}_{nl}^*)^{\mathrm{T}}\boldsymbol{\sigma} > \\ &= \delta\mathbf{q}_{\tau i}^{\mathrm{T}} < \mathrm{diag}\left[(\mathbf{B}_{nl}^*)^{\mathrm{T}}\boldsymbol{\sigma}\right] > \mathrm{d}\mathbf{q}_{sj} \\ &= \delta\mathbf{q}_{\tau i}^{\mathrm{T}} < \mathrm{diag}\left[(\mathbf{B}_{nl}^*)^{\mathrm{T}}(\boldsymbol{\sigma}_l + \boldsymbol{\sigma}_{nl})\right] > \mathrm{d}\mathbf{q}_{sj} \\ &= \delta\mathbf{q}_{\tau i}^{\mathrm{T}}(\mathbf{K}_{\sigma_l}^{ij\tau s} + \mathbf{K}_{\sigma_{nl}}^{ij\tau s})\mathrm{d}\mathbf{q}_{sj} \\ &= \delta\mathbf{q}_{\tau i}^{\mathrm{T}}\mathbf{K}_\sigma^{ij\tau s}\mathrm{d}\mathbf{q}_{sj} \end{aligned} \tag{14}$$

where the diagonal terms of the 3×3 diagonal matrix $\mathrm{diag}\left[(\mathbf{B}_{nl}^*)^{\mathrm{T}}\boldsymbol{\sigma}\right]$ are the components of the vector $(\mathbf{B}_{nl}^*)^{\mathrm{T}}\boldsymbol{\sigma}$. We have $\boldsymbol{\sigma}_l = \mathbf{C}\boldsymbol{\epsilon}_l$, $\boldsymbol{\sigma}_{nl} = \mathbf{C}\boldsymbol{\epsilon}_{nl}$, and $\mathbf{K}_\sigma^{ij\tau s} = \mathbf{K}_{\sigma_l}^{ij\tau s} + \mathbf{K}_{\sigma_{nl}}^{ij\tau s}$.

More information about the mentioned geometrically nonlinear method are provided by [37, 38, 39]. Furthermore, explicit forms of tangent and secant stiffness matrices regarding the unified formulation of geometrically nonlinear beam and plate structures are mentioned in [26] and [14], respectively. The FN of the important stiffness matrices are given in the Appendix and particular attention is paid to the terms P_{ij}, which are used to penalize the FE arrays opportunely and give the geometrical nonlinear terms of interest.

4 Numerical results

In this section, the numerical results are presented using the nonlinear method mentioned previously and 2-D CUF for plate structures to evaluate the importance of geometrically nonlinear strain-displacement relations for the various problems under consideration. The nonlinear strain-displacement relations used in the proposed study are mentioned in Table 1 of Section 2. In this regard, first, large-deflection equilibrium curves of square plates under bending with fully clamped (CCCC) edge conditions are presented. The post-buckling behavior of different plates are then investigated. In both sections, the presented model is validated and compared with the previous literature.

4.1 Large-deflection response of square plates

An isotropic square plate is considered for the first analysis case. The plate has a width of $a = b =$ 1.2 m, whereas the thickness-to-width ratios are $h/a = 0.02$ and $h/a = 0.1$ (thin and moderately

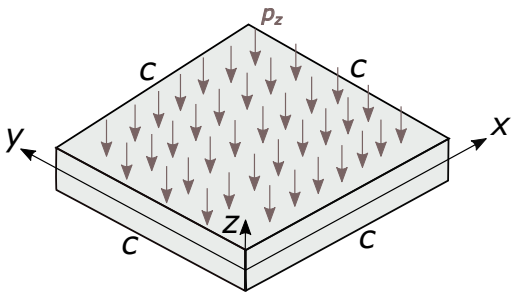

Figure 2: Square plate subjected to uniform pressure

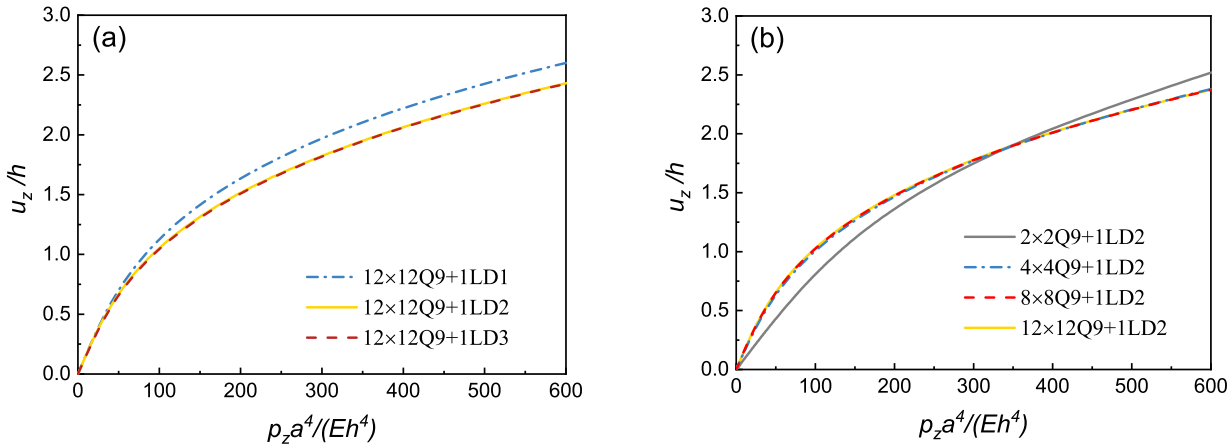

(a) Theory approximations

(b) Mesh sized

Figure 3: Convergence analysis for the CCCC moderately thick plate

thick plates, respectively). The plate is subjected to large deflection due to a transverse uniform pressure and the edges are fully clamped (CCCC). The material is homogeneous with the Young modulus and the Poisson ratio of $E = 75$ GPa and $\nu = 0.3$, respectively. The loading state and the support conditions for this case are shown in Fig. 2.

In this study, mesh sizes and various expansion functions in the thickness direction are considered to carry out the convergence analysis. First, the number of plate elements is fixed at 12x12 Q9 and the analysis is for the investigation of the theory order on the thickness dimension. In the second analysis, the theory approximation order is fixed (LD2), whereas the number of finite elements is varied. The results are shown in Fig. 3 which depicts the vertical displacement at the centroid of the moderately thick plate for different pressure loadings. Based on the results presented in this figure, 12x12 Q9 elements with LD2 CUF plate model are used for the subsequent analyses.

The large-deflection equilibrium curves of a square plate subjected to the uniform pressure are plotted in Fig. 4 based on the full nonlinear, von Kármán, and linear CUF plate models. Furthermore, the results are compared with those available in the literature [11]. The equilibrium curves for both the thin plate ($h/a = 0.02$) and moderately thick plate ($h/a = 0.1$) are shown in Fig. 4. The results show that the presented model of this study can predict large-deflection equilibrium curves accurately. In addition, by the comparison of two illustrated graphs, it could be comprehended that for the case of thin plate, the effect of all geometrically nonlinear strain-displacement relations other than von Kármán theory, is not significant. Therefore, using von Kármán theory in the large-deflection analysis of thin plates is reliable and accurate. However, for the case of moderately thick plate, the discrepancies between the von Kármán theory and the full nonlinear model is significant in the large deflections regime.

In order to evaluate the effects of different nonlinear strain-displacement relations on the equi-

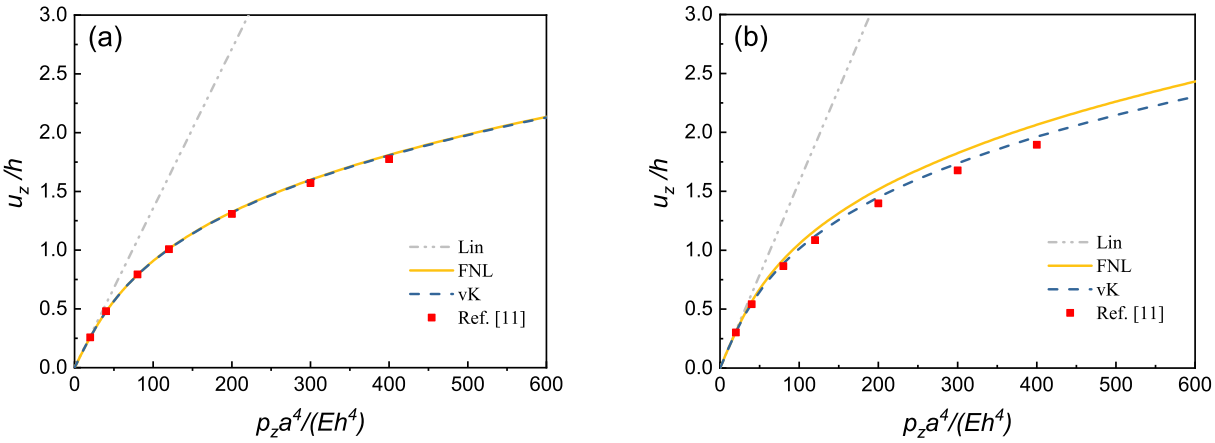

(a) Thin plate ($h/a = 0.02$) (b) Moderately thick plate ($h/a = 0.1$)

Figure 4: Large-deflection equilibrium curves of CCCC square plate

librium curves further, nonlinear analysis is performed based on P_{ij} parameters introduced in the previous section. The results are shown in the graphs of Fig. 5. This figure shows the fact that the Linear theory (Lin) and the full nonlinear theory without von Kármán terms (FNL$_{-vK}$) have the most significant discrepancies in comparison with other investigated theories. In fact, for the case of plate under bending, the difference between the von Kármán theory (vK), the full nonlinear theory (FNL) and the other modifications which include the von Kármán terms (vK$_{+T}$, vK$_{+S}$, vK$_{+IN}$, and vK$_{+All}$), is not so significant.

Also, for the mentioned problem of moderately thick plate under bending, the stress distributions are investigated based on different nonlinear theories. This comparison is done for two states of fixed load and fixed displacement in order to have a better understanding of the effect of different nonlinear strain-displacement relations on the axial and shear stress distributions. First, through-the-thickness distributions of the dimensionless transverse shear stress $\sigma_{xz}a^2/(Eh^2)$ at the point ($x = a/6$, $y = b/2$) of CCCC square plates based on different full nonlinear plate models at the fixed load of $\frac{P_z a^4}{Eh^4} = 200$ are investigated. As illustrated in Fig. 6, LD1 and LD2 models are less accurate in comparison with other ones. In fact, the LD1 and 1LD2 full nonlinear CUF plate models cannot give a physically acceptable distribution of the shear stress, while the other higher order CUF plate models can provide an accurate description of the quadratic shear stress distribution.

Through-the-thickness distributions of the dimensionless in-plane normal stress $\sigma_{xx}a^2/(Eh^2)$ at the middle point ($x = a/2$, $y = b/2$) of CCCC square plates based on different geometrically nonlinear plate models at the fixed load of $\frac{P_z a^4}{Eh^4} = 200$ are shown in Fig. 7 according to LD2 and LD3 plate models. The results show that the difference between the prediction of axial stress for investigated nonlinear theories is not significant for the case of plate under bending. Therefore, both LD2 and LD3 plate models could offer accurate results for all the theories that consider von Kármán terms.

Through-the-thickness distributions of the dimensionless transverse shear stress $\sigma_{xz}a^2/(Eh^2)$ at the point ($x = a/6$, $y = b/2$) of CCCC square plates based on different geometrically nonlinear plate models at the fixed load of $\frac{P_z a^4}{Eh^4} = 200$ are shown in Fig. 8 according to LD2 plate model and LD3 plate model, respectively. The results show that the traction-free boundary condition ($\sigma_{xz} = 0$) of the shear stress at the bottom surface ($z = -h/2$) is satisfied by the 1LD3 nonlinear plate model. Note that the shear stress is not null at z/h=0.5, because of the fact that in the large displacement regime the applied pressure has a component parallel to the plate top surface (conservative problem).

In the subsequent analysis, the effect on stress distribution of different approximation order and geometric nonlinear approximation is investigated in the case of fixed displacement of $\frac{u_z}{h} = 1.5$. In

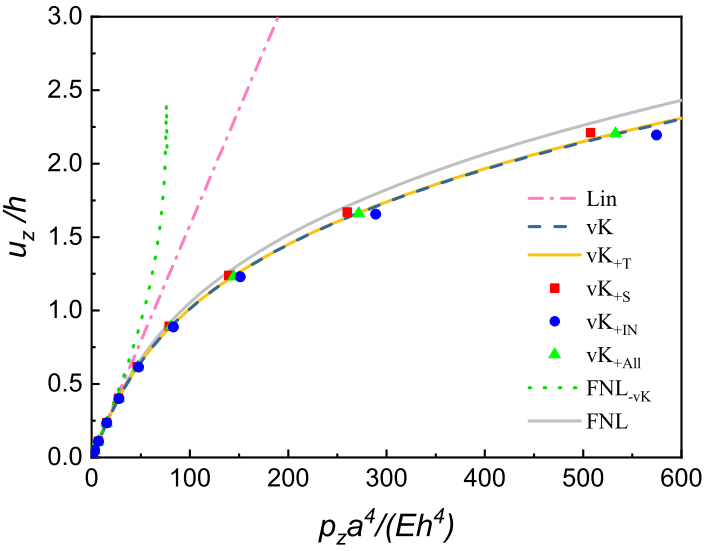

Figure 5: Effect of nonlinear strain-displacement relations on the equilibrium curves in the case of CCCC moderately thick square plate under uniform pressure

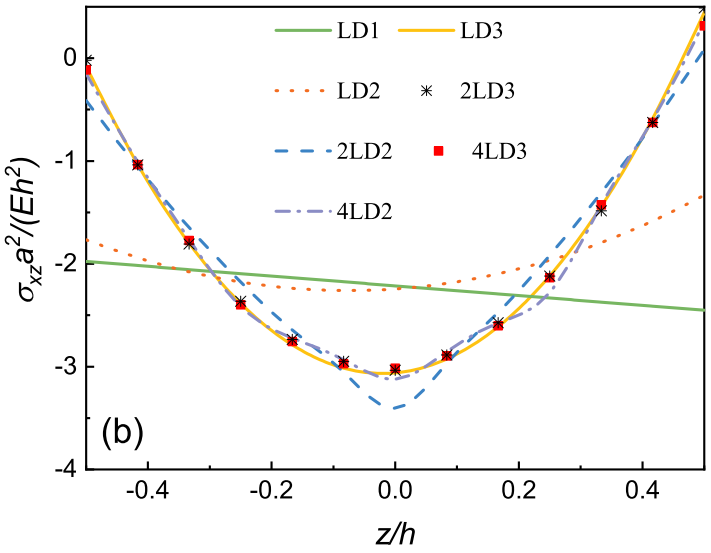

Figure 6: Through-the-thickness distributions of the dimensionless transverse shear stress $\sigma_{xz}a^2/(Eh^2)$ at the point $(x = a/6,\ y = b/2)$ of CCCC moderately thick square plates based on different full nonlinear plate models at the fixed load of $\frac{P_z a^4}{Eh^4} = 200$

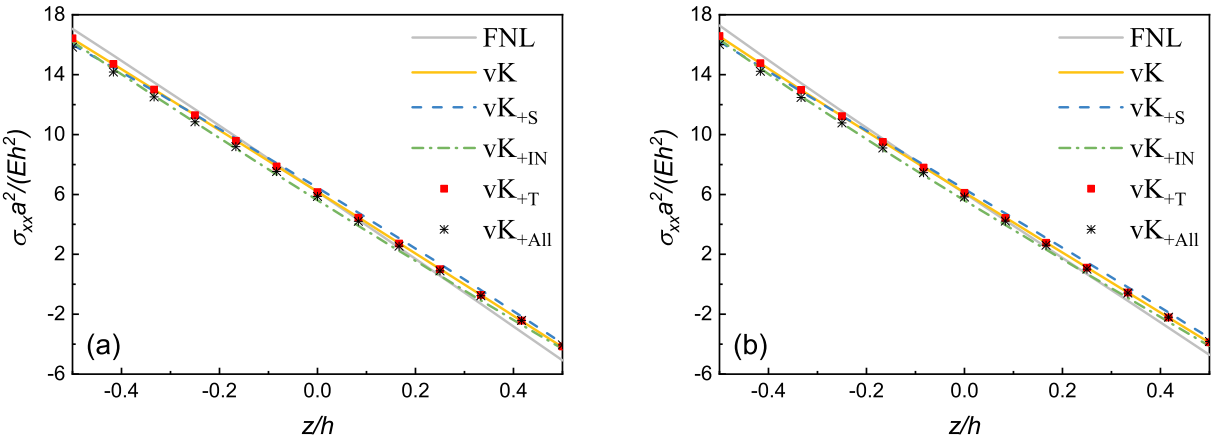

(a) LD2 plate model ($h/a = 0.02$)

(b) LD3 plate model ($h/a = 0.1$)

Figure 7: Through-the-thickness distributions of the dimensionless in-plane normal stress $\sigma_{xx}a^2/(Eh^2)$ at the middle point ($x = a/2$, $y = b/2$) of CCCC moderately thick square plates based on different geometrically nonlinear plate models at the fixed load of $\frac{P_z a^4}{Eh^4} = 200$

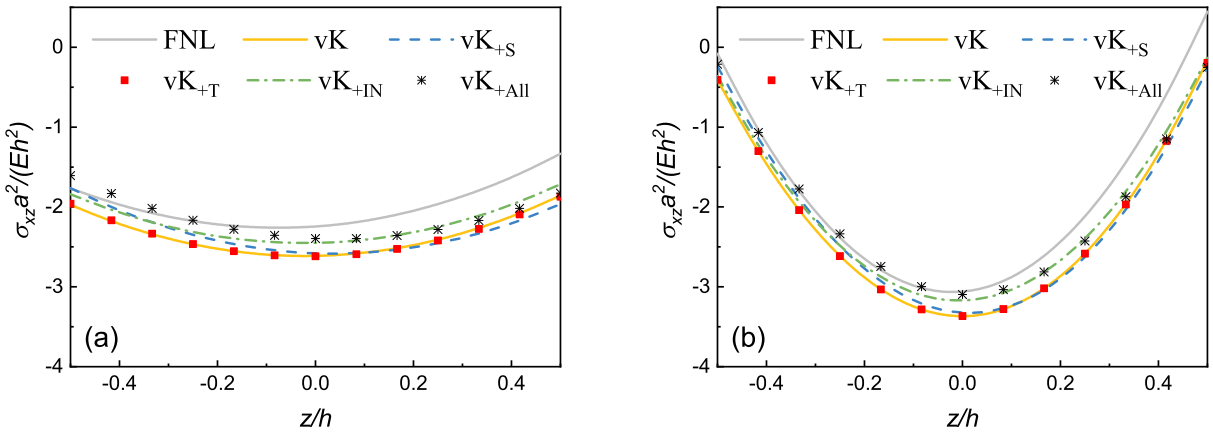

(a) LD2 plate model

(b) LD3 plate model

Figure 8: Through-the-thickness distributions of the dimensionless transverse shear stress $\sigma_{xz}a^2/(Eh^2)$ at the point ($x = a/6$, $y = b/2$) of CCCC moderately thick square plates based on different geometrically nonlinear plate models at the fixed load of $\frac{P_z a^4}{Eh^4} = 200$

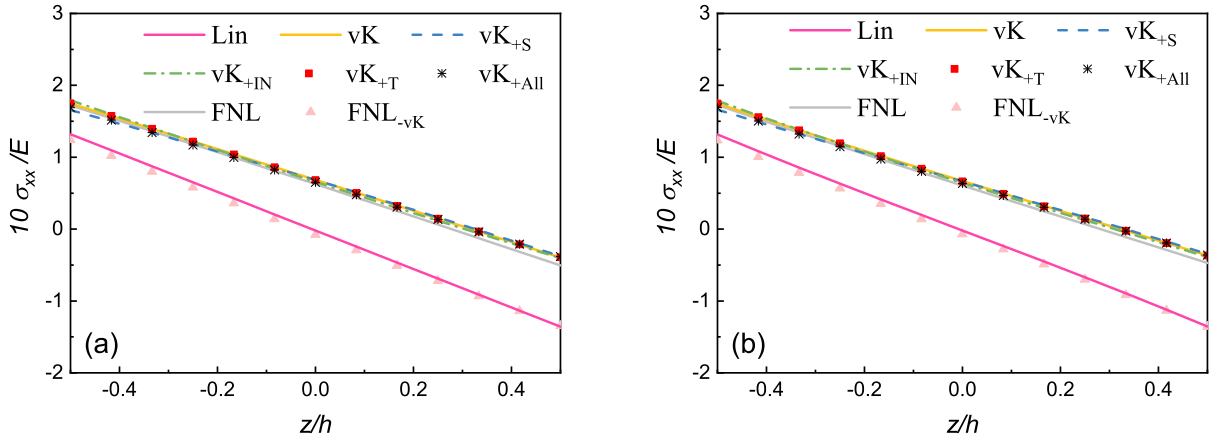

(a) LD2 plate model

(b) LD3 plate model

Figure 9: Through-the-thickness distributions of the dimensionless in-plane normal stress $\frac{10\sigma_{xx}}{E}$ at the middle point ($x = a/2$, $y = b/2$) of CCCC moderately thick square plates based on different geometrically nonlinear plate models at the fixed displacement of $\frac{u_z}{h} = 1.5$

this case, the linear theory (Lin) and the full nonlinear theory without von Kármán terms (FNL_{-vK}) are also considered for the comparison of stress distributions (see Fig. 5). Through-the-thickness distributions of the dimensionless in-plane normal stress $\frac{10\sigma_{xx}}{E}$ at the middle point ($x = a/2$, $y = b/2$) of CCCC square plates based on different geometrically nonlinear plate models at the fixed displacement of $\frac{u_z}{h} = 1.5$ are shown in Fig. 9 according to LD2 plate model and LD3 plate model, respectively. This figure shows the fact that the linear theory and the full nonlinear theories without von Kármán terms have the most significant discrepancies in comparison with other investigated theories. It can also be understood from the figure, that for the case of plate under bending, the difference between the predictions of shear stress for the von Kármán theory, the full nonlinear theory and the other modifications which include the von Kármán terms, is not so significant.

The through-the-thickness distributions of the dimensionless transverse shear stress $\frac{100\sigma_{xz}}{E}$ at the point ($x = a/6$, $y = b/2$) of CCCC square plates based on different geometrically nonlinear plate models at the fixed displacement of $\frac{u_z}{h} = 1.5$ are shown in Fig. 10 according to the LD2 and LD3 plate models, respectively. The results show that the traction-free boundary condition ($\sigma_{xz} = 0$) of the shear stress at the bottom surface ($z = -h/2$) is satisfied by the 1LD3 nonlinear plate model. In addition, except for the full nonlinear theory, the discrepancies between the shear stress predictions of other investigated nonlinear theories is not so significant.

4.2 Post-buckling analysis of slender plates

In this section, the post-buckling analysis of slender plates is presented based on different support conditions and loading states for various nonlinear strain-displacement relations. For the first case, width and thickness of the slender plates are $a = 30$ cm, $b = 6$ cm and $h = 0.6$ cm, respectively. For the clamped edge condition $u = v = w = 0$ at $x = 0$. On the other hand, for the immovable simply-supported edge condition $u = v = w = 0$ at $z = 0$ and $x = 0$. In addition, movable simply-supported edge condition 'S_1' satisfies $v = w = 0$ at $z = 0$ and $x = a$. The point compression load is applied at the point ($x = a$, $y = b/2$, $z = 0$) and a small defection load is used to produce a stable post-buckling nonlinear response. The material is homogeneous with the Young modulus and Poisson ratio of $E = 75$ GPa and $\nu = 0.316$, respectively.

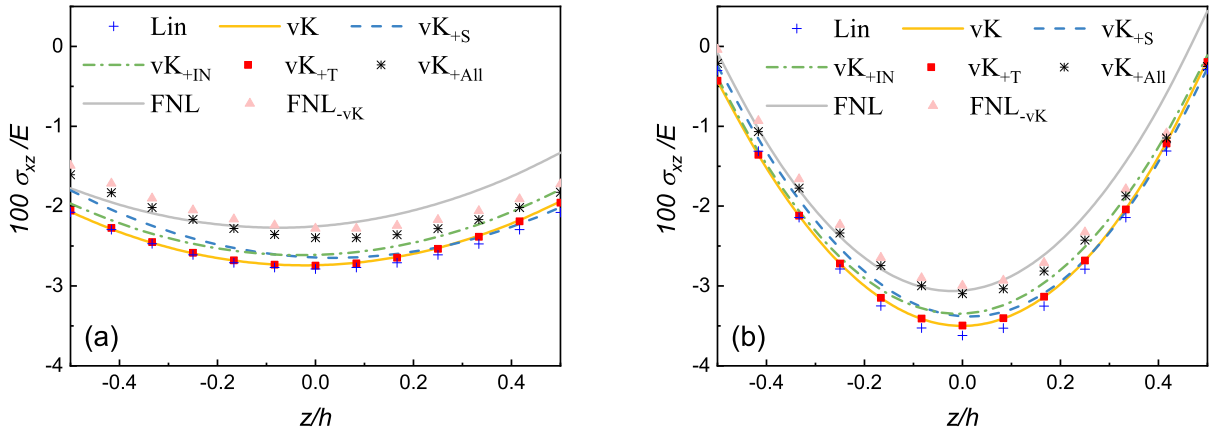

(a) LD2 plate model

(b) LD3 plate model

Figure 10: Through-the-thickness distributions of the dimensionless transverse shear stress $\frac{100\sigma_{xz}}{E}$ at the point $(x = a/6,\ y = b/2)$ of CCCC moderately thick square plates based on different geometrically nonlinear plate models at the fixed displacement of $\frac{u_z}{h} = 1.5$

4.2.1 Validation

In this section, the post-buckling equilibrium curves from the LD2 full nonlinear and the von Kármán are compared with those from refined CUF beam models, which have been already widely validated in [14, 26, 28]. The first plate case has one clamped edge and three free edges (CFFF), while the second one has two immovable simply-supported and movable simply-supported edges in the opposite direction and two other free edges (SFS_1F). As illustrated in Fig. 11, the equilibrium curves are demonstrated to be accurate and well correlated for both beam cases and slender plates. In addition, it is evident from the figure that the von Kármán theory cannot predict the equilibrium curves effectively in the beam model or in the plate LD2 model.

4.2.2 Post-buckling of slender plates with the (movable simply-supported)-free-(movable simply-supported)-free (S_1FS_1F) edge conditions

In this section, the post-buckling equilibrium curves and stress distributions of slender plate under the in-plane compressive point loads is investigated. The slender plate has the length, width and thickness of $a = 20$ cm, $b = 5$ cm, and $h = 0.4$ cm, respectively. The edge conditions for this case are (movable simply-supported)-free-(movable simply-supported)-free (S_1FS_1F). The post-buckling equilibrium curves of this case are shown in Fig. 12 based on different geometrically nonlinear CUF plate models. The results show the fact that for this case, only the full nonlinear model offers reliable and accurate results. In fact, for this case the von Kármán theory and all other modifications cannot predict the post-buckling equilibrium curves correctly.

In order to have a better understanding of the effect of different nonlinear strain-displacement relations on the axial and shear stress distributions, the stress distributions for this case are compared based on the investigated nonlinear theories. The through-the-thickness distributions of the dimensionless transverse shear stress $\sigma_{xz}h^2/P$ at the point $(x = a/4,\ y = b/4)$ of S_1FS_1F slender plates based on different full nonlinear plate models at the fixed load of $\frac{Pa^2}{\pi^2 E l_b} = 1.1$ are presented in Fig. 13. As illustrated in this figure, the LD2 model is less accurate in comparison with other models. In fact, the LD2 full nonlinear CUF plate model cannot give a physically acceptable distribution of the shear stress, while the other plate models can provide an accurate description of the shear stress distribution.

Through-the-thickness distributions of the dimensionless in-plane normal stress $\sigma_{xx}bh^2/(Pa)$ at

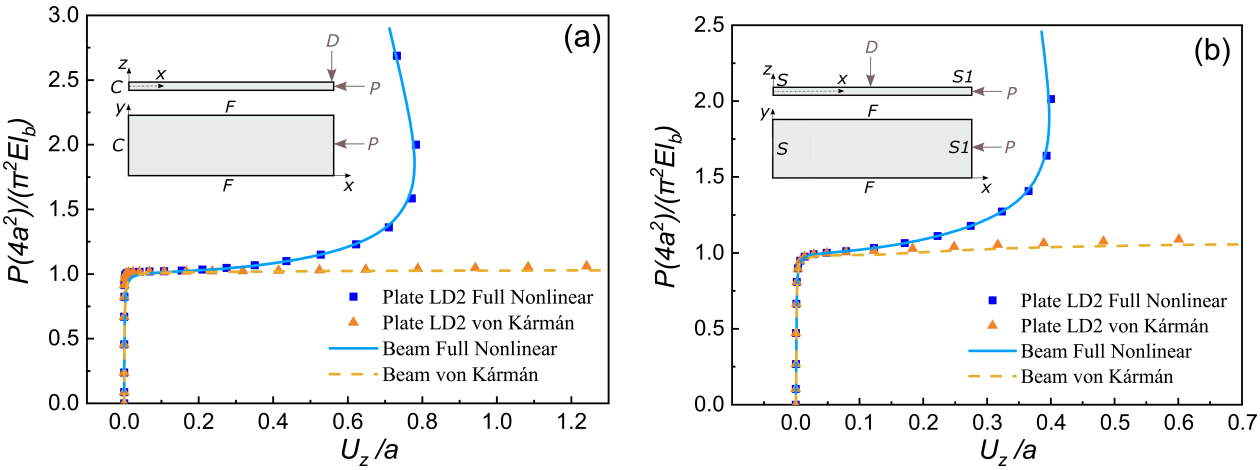

(a) One clamped edge and three free edges (CFFF)

(b) (Immovable simply-supported)-free-(movable simply-supported)-free (SFS_1F)

Figure 11: Post-buckling equilibrium curves for slender plates subjected to an in-plane compressive point load P based on plate and beam models (a) one clamped edge and three free edges (CFFF), (b) (immovable simply-supported)-free-(movable simply-supported)-free (SFS_1F)

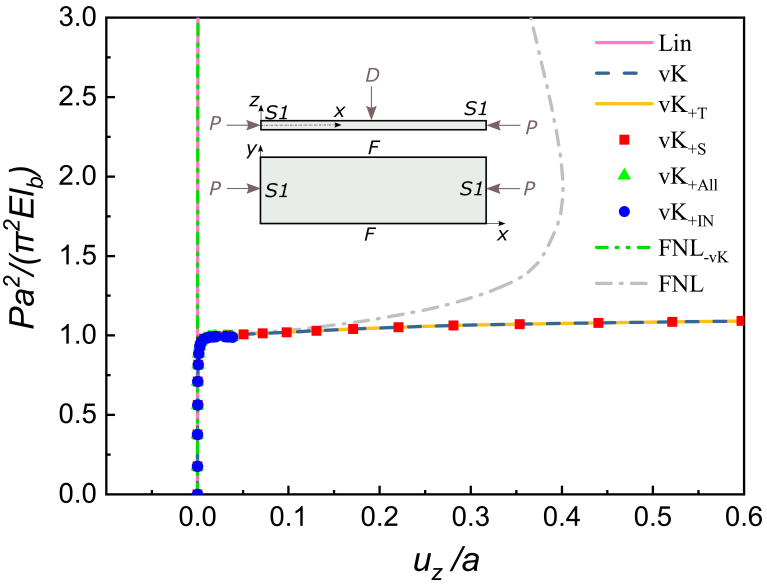

Figure 12: Post-buckling equilibrium curves of slender plates under the in-plane compressive point loads for the (movable simply-supported)-free-(movable simply-supported)-free (S_1FS_1F) edge conditions based on different geometrically nonlinear CUF plate models

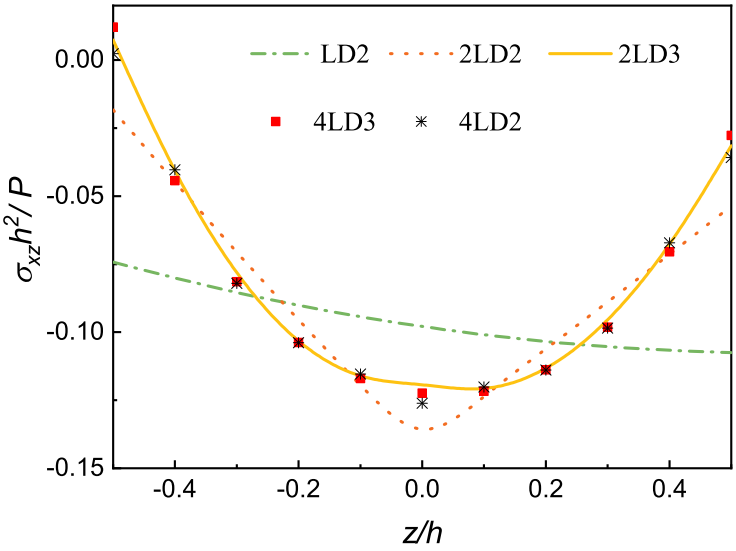

Figure 13: Through-the-thickness distributions of the dimensionless transverse shear stress $\sigma_{xz}h^2/P$ at the point ($x = a/4$, $y = b/4$) of S_1FS_1F slender plates based on different full nonlinear plate models at the fixed load of $\frac{Pa^2}{\pi^2 E l_b} = 1.1$

the point ($x = a/4$, $y = b/4$) of S_1FS_1F slender plates based on different geometrically nonlinear plate models at the fixed load of $\frac{Pa^2}{\pi^2 E l_b} = 1.1$ are shown in Fig. 14 according to the LD2 plate model and the LD3 plate model, respectively. The results show the fact that for this case of post-buckling, only the full nonlinear model offers reliable and accurate results. In fact, for this case, neither the von Kármán theory nor any other modifications can predict the axial stress distributions correctly. It is also comprehended from the graphs that the selection of LD2 or 2LD3 does not influence the results of axial stress considerably.

The through-the-thickness distributions of the dimensionless transverse shear stress $\sigma_{xz}h^2/P$ at the point ($x = a/4$, $y = b/4$) of S_1FS_1F slender plates based on different geometrically nonlinear plate models at the fixed load of $\frac{Pa^2}{\pi^2 E l_b} = 1.1$ are shown in Fig. 15 according to the LD2 plate model and the LD3 plate model, respectively. The results show the fact that, the difference between shear stress results obtained by the full nonlinear theory and the other nonlinear plate theories such as the von Kármán and its modifications is considerable. Furthermore, the linear theory and the full nonlinear theory without von Kármán terms cannot predict the shear stress distributions for either the LD2 or 2LD3 plate models.

4.2.3 Post-buckling of slender plates with all edges simply-supported ($S_1S_2S_1S_2$)

In order to investigate the effect of edge and loading conditions on the post-buckling behavior of plates, the equilibrium curves of slender plate in the previous section is considered with all the plate edges simply-supported and a line compression load shown in Fig. 16. The resultant force of P is applied at the middle-line of the cross section. Note that simply-supported edge conditions along the length satisfy $w = 0$ at $z = 0$ and $y = 0, b$. Post-buckling nonlinear response of the slender plate based on different nonlinear strain-displacement relations for this case is shown in Fig. 16. For this case, the results show the fact that only the full nonlinear model offers reliable and accurate results. However, the difference between the other full nonlinear theories such as the von Kármán theory and other modifications is not as significant as the previous section 4.2.2 (see Fig. 12). Actually, for this case the von Kármán theory and all other modifications cannot predict the post-buckling equilibrium curves accurately and precisely as the full nonlinear theory. As a result, the assumption of geometric nonlinear relations based on the edge and loading conditions of the plate structure can

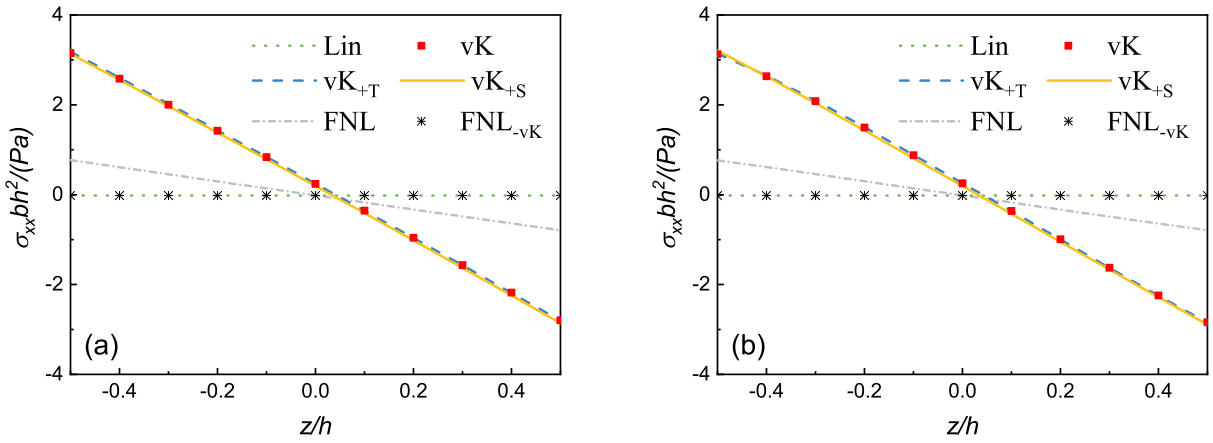

(a) LD2 plate model

(b) 2LD3 plate model

Figure 14: Through-the-thickness distributions of the dimensionless in-plane normal stress $\sigma_{xx}bh^2/(Pa)$ at the point $(x = a/4,\ y = b/4)$ of S_1FS_1F slender plates based on different geometrically nonlinear plate models at the fixed load of $\frac{Pa^2}{\pi^2 El_b} = 1.1$

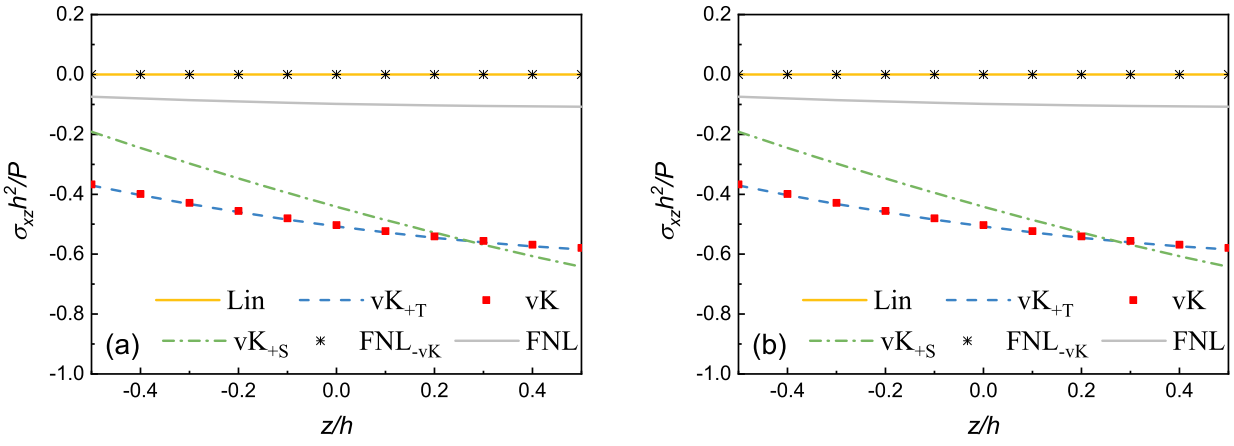

(a) LD2 plate model

(b) 2LD3 plate model

Figure 15: Through-the-thickness distributions of the dimensionless transverse shear stress $\sigma_{xz}h^2/P$ at the point $(x = a/4,\ y = b/4)$ of S_1FS_1F slender plates based on different geometrically nonlinear plate models at the fixed load of $\frac{Pa^2}{\pi^2 El_b} = 1.1$

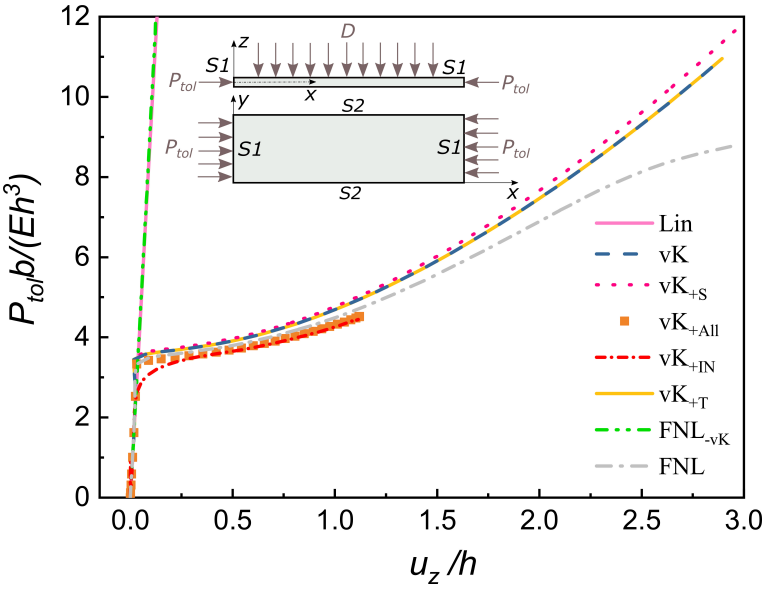

Figure 16: Post-buckling equilibrium curves of slender plates with all edges simply-supported ($S_1S_2S_1S_2$) under the in-plane compressive line loads based on different geometrically nonlinear CUF plate models

influence post-buckling curves significantly.

5 Conclusions

In this paper, the large-deflection and post-buckling of rectangular plates have been studied using CUF. This framework has provided us with the ability to consider different geometric nonlinear relations. Therefore, the well-known von Kármán theory for nonlinear deformations of plates has been investigated with different modifications such as the thickness stretching and shear deformations due to transverse deflection. In this regard, equilibrium curves and related stress distributions for each case heve been presented and discussed. For the case of a plate under bending with CCCC edge conditions, the equilibrium curves have been compared successfully with the available literature for both thin plate and moderately thick plate. The equilibrium curves and the obtained stress distributions have shown the fact that the consideration of different geometric nonlinear relations for the moderately thick plates is more sensitive compared to the thin plates. Therefore, different modifications other than von Kármán theory should be considered for the large deflections of thick and moderately thick plates. Post-buckling behavior of plates has also been focused on and discussed based on different nonlinear strain-displacement assumptions. It has been shown that for the case of slender plates under the in-plane compressive point loads with the (movable simply-supported)-free-(movable simply-supported)-free edge conditions, only full Green-Lagrange nonlinear model can predict the nonlinear behavior of plates efficiently and accurately, while other approximations produce considerable inaccuracies. In addition, for the post-buckling equilibrium curves of slender plates with all edges simply-supported under in-plane compressive line loads, the results have been more sensitive to the selected strain-displacement relations.

Appendix A Components of the secant stiffness matrix based on parameters of P_{ij}

The nine components of the FN of the first-order nonlinear stiffness matrix $\mathbf{K}_{nll}^{ij\tau s}(r,c)$ can be derived as

For $c=1$:

$$\begin{aligned}
\mathbf{K}_{nll}^{ij\tau s}[r,1] &= < P_{11}\mathbf{u}_{,x}[r]\, C_{11}\, F_\tau\, F_s\, N_{i,_x}\, N_{j,_x} > + < P_{41}\mathbf{u}_{,x}[r]\, C_{44}\, F_{\tau,_z}\, F_{s,_z}\, N_i\, N_j > \\
&+ < P_{61}\mathbf{u}_{,x}[r]\, C_{66}\, F_\tau\, F_s\, N_{i,_y}\, N_{j,_y} > + < P_{61}\mathbf{u}_{,x}[r]\, C_{16}\, F_\tau\, F_s\, N_{i,_y}\, N_{j,_x} > \\
&+ < P_{11}\mathbf{u}_{,x}[r]\, C_{16}\, F_\tau\, F_s\, N_{i,_x}\, N_{j,_y} > + < P_{61}\mathbf{u}_{,y}[r]\, C_{66}\, F_\tau\, F_s\, N_{i,_x}\, N_{j,_y} > \\
&+ < P_{21}\mathbf{u}_{,y}[r]\, C_{12}\, F_\tau\, F_s\, N_{i,_y}\, N_{j,_x} > + < P_{51}\mathbf{u}_{,y}[r]\, C_{45}\, F_{\tau,_z}\, F_{s,_z}\, N_i\, N_j > \\
&+ < P_{61}\mathbf{u}_{,y}[r]\, C_{16}\, F_\tau\, F_s\, N_{i,_x}\, N_{j,_x} > + < P_{21}\mathbf{u}_{,y}[r]\, C_{26}\, F_\tau\, F_s\, N_{i,_y}\, N_{j,_y} > \\
&+ < P_{41}\mathbf{u}_{,z}[r]\, C_{44}\, F_\tau\, F_{s,_z}\, N_{i,_x}\, N_j > + < P_{31}\mathbf{u}_{,z}[r]\, C_{13}\, F_{\tau,_z}\, F_s\, N_i\, N_{j,_x} > \\
&+ < P_{51}\mathbf{u}_{,z}[r]\, C_{45}\, F_\tau\, F_{s,_z}\, N_{i,_y}\, N_j > + < P_{31}\mathbf{u}_{,z}[r]\, C_{36}\, F_{\tau,_z}\, F_s\, N_i\, N_{j,_y} >,
\end{aligned}$$

For $c=2$:

$$\begin{aligned}
\mathbf{K}_{nll}^{ij\tau s}[r,2] &= < P_{11}\mathbf{u}_{,x}[r]\, C_{12}\, F_\tau\, F_s\, N_{i,_x}\, N_{j,_y} > + < P_{61}\mathbf{u}_{,x}[r]\, C_{66}\, F_\tau\, F_s\, N_{i,_y}\, N_{j,_x} > \\
&+ < P_{41}\mathbf{u}_{,x}[r]\, C_{45}\, F_{\tau,_z}\, F_{s,_z}\, N_i\, N_j > + < P_{11}\mathbf{u}_{,x}[r]\, C_{16}\, F_\tau\, F_s\, N_{i,_x}\, N_{j,_x} > \\
&+ < P_{61}\mathbf{u}_{,x}[r]\, C_{26}\, F_\tau\, F_s\, N_{i,_y}\, N_{j,_y} > + < P_{61}\mathbf{u}_{,y}[r]\, C_{66}\, F_\tau\, F_s\, N_{i,_x}\, N_{j,_x} > \\
&+ < P_{51}\mathbf{u}_{,y}[r]\, C_{55}\, F_{\tau,_z}\, F_{s,_z}\, N_i\, N_j > + < P_{21}\mathbf{u}_{,y}[r]\, C_{22}\, F_\tau\, F_s\, N_{i,_y}\, N_{j,_y} > \\
&+ < P_{21}\mathbf{u}_{,y}[r]\, C_{26}\, F_\tau\, F_s\, N_{i,_y}\, N_{j,_x} > + < P_{61}\mathbf{u}_{,y}[r]\, C_{26}\, F_\tau\, F_s\, N_{i,_x}\, N_{j,_y} > \\
&+ < P_{31}\mathbf{u}_{,z}[r]\, C_{23}\, F_{\tau,_z}\, F_s\, N_i\, N_{j,_y} > + < P_{51}\mathbf{u}_{,z}[r]\, C_{55}\, F_\tau\, F_{s,_z}\, N_{i,_y}\, N_j > \\
&+ < P_{41}\mathbf{u}_{,z}[r]\, C_{45}\, F_\tau\, F_{s,_z}\, N_{i,_x}\, N_j > + < P_{31}\mathbf{u}_{,z}[r]\, C_{36}\, F_{\tau,_z}\, F_s\, N_i\, N_{j,_x} >,
\end{aligned}$$

For $c=3$:

$$\begin{aligned}
\mathbf{K}_{nll}^{ij\tau s}[r,3] &= < P_{11}\mathbf{u}_{,x}[r]\, C_{13}\, F_\tau\, F_{s,_z}\, N_{i,_x}\, N_j > + < P_{41}\mathbf{u}_{,x}[r]\, C_{44}\, F_{\tau,_z}\, F_s\, N_i\, N_{j,_x} > \\
&+ < P_{41}\mathbf{u}_{,x}[r]\, C_{45}\, F_{\tau,_z}\, F_s\, N_i\, N_{j,_y} > + < P_{61}\mathbf{u}_{,x}[r]\, C_{36}\, F_\tau\, F_{s,_z}\, N_{i,_y}\, N_j > \\
&+ < P_{51}\mathbf{u}_{,y}[r]\, C_{55}\, F_{\tau,_z}\, F_s\, N_i\, N_{j,_y} > + < P_{21}\mathbf{u}_{,y}[r]\, C_{23}\, F_\tau\, F_{s,_z}\, N_{i,_y}\, N_j > \\
&+ < P_{51}\mathbf{u}_{,y}[r]\, C_{45}\, F_{\tau,_z}\, F_s\, N_i\, N_{j,_x} > + < P_{61}\mathbf{u}_{,y}[r]\, C_{36}\, F_\tau\, F_{s,_z}\, N_{i,_x}\, N_j > \\
&+ < P_{41}\mathbf{u}_{,z}[r]\, C_{44}\, F_\tau\, F_s\, N_{i,_x}\, N_{j,_x} > + < P_{31}\mathbf{u}_{,z}[r]\, C_{33}\, F_{\tau,_z}\, F_{s,_z}\, N_i\, N_j > \\
&+ < P_{51}\mathbf{u}_{,z}[r]\, C_{55}\, F_\tau\, F_s\, N_{i,_y}\, N_{j,_y} > + < P_{41}\mathbf{u}_{,z}[r]\, C_{45}\, F_\tau\, F_s\, N_{i,_x}\, N_{j,_y} > \\
&+ < P_{51}\mathbf{u}_{,z}[r]\, C_{45}\, F_\tau\, F_s\, N_{i,_y}\, N_{j,_x} > .
\end{aligned}$$

The nine components of $\mathbf{K}_{lnl}^{ij\tau s}$ can be easily obtained from Eq. $\left(\mathbf{K}_{lnl}^{ij\tau s}\right)^{\mathrm{T}} = \mathbf{K}_{nll}^{jis\tau}/2$.

Finally, the nine components of the matrix $\mathbf{K}^{ij\tau s}_{nlnl}[r,c]$ are provided in the following:

$$
\begin{aligned}
2\times \mathbf{K}^{ij\tau s}_{nlnl}[r,c] \;=\;& < P_{11}P_{11}\mathbf{u}_{,x}[r]\,\mathbf{u}_{,x}[c]\; C_{11}\,F_\tau\,F_s\,N_{i_{,x}}\,N_{j_{,x}} > + < P_{41}P_{41}\mathbf{u}_{,x}[r]\,\mathbf{u}_{,x}[c]\,C_{44}\,F_{\tau_{,z}}\,F_{s_{,z}}\,N_i\,N_j > \\
+\;& < P_{61}P_{61}\mathbf{u}_{,x}[r]\,\mathbf{u}_{,x}[c]\,C_{66}\,F_\tau\,F_s\,N_{i_{,y}}\,N_{j_{,y}} > + < P_{11}P_{61}\mathbf{u}_{,x}[r]\,\mathbf{u}_{,x}[c]\,C_{16}\,F_\tau\,F_s\,N_{i_{,x}}\,N_{j_{,y}} > \\
+\;& < P_{11}P_{61}\mathbf{u}_{,x}[r]\,\mathbf{u}_{,x}[c]\,C_{16}\,F_\tau\,F_s\,N_{i_{,y}}\,N_{j_{,x}} > + < P_{61}P_{61}\mathbf{u}_{,y}[r]\,\mathbf{u}_{,y}[c]\;C_{66}\,F_\tau\,F_s\,N_{i_{,x}}\,N_{j_{,x}} > \\
+\;& < P_{51}P_{51}\mathbf{u}_{,y}[r]\,\mathbf{u}_{,y}[c]\,C_{55}\,F_{\tau_{,z}}\,F_{s_{,z}}\,N_i\,N_j > + < P_{21}P_{21}\mathbf{u}_{,y}[r]\,\mathbf{u}_{,y}[c]\,C_{22}\,F_\tau\,F_s\,N_{i_{,y}}\,N_{j_{,y}} > \\
+\;& < P_{21}P_{61}\mathbf{u}_{,y}[r]\,\mathbf{u}_{,y}[c]\,C_{26}\,F_\tau\,F_s\,N_{i_{,x}}\,N_{j_{,y}} > + < P_{21}P_{61}\mathbf{u}_{,y}[r]\,\mathbf{u}_{,y}[c]\,C_{26}\,F_\tau\,F_s\,N_{i_{,y}}\,N_{j_{,x}} > \\
+\;& < P_{41}P_{41}\mathbf{u}_{,z}[r]\,\mathbf{u}_{,z}[c]\;C_{44}\,F_\tau\,F_s\,N_{i_{,x}}\,N_{j_{,x}} > + < P_{31}P_{31}\mathbf{u}_{,z}[r]\,\mathbf{u}_{,z}[c]\,C_{33}\,F_{\tau_{,z}}\,F_{s_{,z}}\,N_i\,N_j > \\
+\;& < P_{51}P_{51}\mathbf{u}_{,z}[r]\,\mathbf{u}_{,z}[c]\,C_{55}\,F_\tau\,F_s\,N_{i_{,y}}\,N_{j_{,y}} > + < P_{41}P_{51}\mathbf{u}_{,z}[r]\,\mathbf{u}_{,z}[c]\,C_{45}\,F_\tau\,F_s\,N_{i_{,x}}\,N_{j_{,y}} > \\
+\;& < P_{41}P_{51}\mathbf{u}_{,z}[r]\,\mathbf{u}_{,z}[c]\,C_{45}\,F_\tau\,F_s\,N_{i_{,y}}\,N_{j_{,x}} > + < P_{11}P_{21}\mathbf{u}_{,x}[r]\,\mathbf{u}_{,y}[c]\,C_{12}\,F_\tau\,F_s\,N_{i_{,x}}\,N_{j_{,y}} > \\
+\;& < P_{61}P_{61}\mathbf{u}_{,x}[r]\,\mathbf{u}_{,y}[c]\,C_{66}\,F_\tau\,F_s\,N_{i_{,y}}\,N_{j_{,x}} > + < P_{41}P_{51}\mathbf{u}_{,x}[r]\,\mathbf{u}_{,y}[c]\,C_{45}\,F_{\tau_{,z}}\,F_{s_{,z}}\,N_i\,N_j > \\
+\;& < P_{11}P_{61}\mathbf{u}_{,x}[r]\,\mathbf{u}_{,y}[c]\,C_{16}\,F_\tau\,F_s\,N_{i_{,x}}\,N_{j_{,x}} > + < P_{21}P_{61}\mathbf{u}_{,x}[r]\,\mathbf{u}_{,y}[c]\,C_{26}\,F_\tau\,F_s\,N_{i_{,y}}\,N_{j_{,y}} > \\
+\;& < P_{11}P_{21}\mathbf{u}_{,y}[r]\,\mathbf{u}_{,x}[c]\,C_{12}\,F_\tau\,F_s\,N_{i_{,y}}\,N_{j_{,x}} > + < P_{61}P_{61}\mathbf{u}_{,y}[r]\,\mathbf{u}_{,x}[c]\,C_{66}\,F_\tau\,F_s\,N_{i_{,x}}\,N_{j_{,y}} > \\
+\;& < P_{41}P_{51}\mathbf{u}_{,y}[r]\,\mathbf{u}_{,x}[c]\,C_{45}\,F_{\tau_{,z}}\,F_{s_{,z}}\,N_i\,N_j > + < P_{11}P_{61}\mathbf{u}_{,y}[r]\,\mathbf{u}_{,x}[c]\,C_{16}\,F_\tau\,F_s\,N_{i_{,x}}\,N_{j_{,x}} > \\
+\;& < P_{21}P_{61}\mathbf{u}_{,y}[r]\,\mathbf{u}_{,x}[c]\,C_{26}\,F_\tau\,F_s\,N_{i_{,y}}\,N_{j_{,y}} > + < P_{11}P_{31}\mathbf{u}_{,x}[r]\,\mathbf{u}_{,z}[c]\,C_{13}\,F_\tau\,F_{s_{,z}}\,N_{i_{,x}}\,N_j > \\
+\;& < P_{41}P_{41}\mathbf{u}_{,x}[r]\,\mathbf{u}_{,z}[c]\,C_{44}\,F_{\tau_{,z}}\,F_s\,N_i\,N_{j_{,x}} > + < P_{41}P_{51}\mathbf{u}_{,x}[r]\,\mathbf{u}_{,z}[c]\,C_{45}\,F_{\tau_{,z}}\,F_s\,N_i\,N_{j_{,y}} > \\
+\;& < P_{31}P_{61}\mathbf{u}_{,x}[r]\,\mathbf{u}_{,z}[c]\,C_{36}\,F_\tau\,F_{s_{,z}}\,N_{i_{,y}}\,N_j > + < P_{11}P_{31}\mathbf{u}_{,z}[r]\,\mathbf{u}_{,x}[c]\,C_{13}\,F_{\tau_{,z}}\,F_s\,N_i\,N_{j_{,x}} > \\
+\;& < P_{41}P_{41}\mathbf{u}_{,z}[r]\,\mathbf{u}_{,x}[c]\,C_{44}\,F_\tau\,F_{s_{,z}}\,N_{i_{,x}}\,N_j > + < P_{41}P_{51}\mathbf{u}_{,z}[r]\,\mathbf{u}_{,x}[c]\,C_{45}\,F_\tau\,F_{s_{,z}}\,N_{i_{,y}}\,N_j > \\
+\;& < P_{31}P_{61}\mathbf{u}_{,z}[r]\,\mathbf{u}_{,x}[c]\,C_{36}\,F_{\tau_{,z}}\,F_s\,N_i\,N_{j_{,y}} > + < P_{21}P_{31}\mathbf{u}_{,y}[r]\,\mathbf{u}_{,z}[c]\,C_{23}\,F_\tau\,F_{s_{,z}}\,N_{i_{,y}}\,N_j > \\
+\;& < P_{51}P_{51}\mathbf{u}_{,y}[r]\,\mathbf{u}_{,z}[c]\,C_{55}\,F_{\tau_{,z}}\,F_s\,N_i\,N_{j_{,y}} > + < P_{41}P_{51}\mathbf{u}_{,y}[r]\,\mathbf{u}_{,z}[c]\,C_{45}\,F_{\tau_{,z}}\,F_s\,N_i\,N_{j_{,x}} > \\
+\;& < P_{31}P_{61}\mathbf{u}_{,z}[r]\,\mathbf{u}_{,y}[c]\,C_{36}\,F_\tau\,F_{s_{,z}}\,N_{i_{,x}}\,N_j > + < P_{51}P_{51}\mathbf{u}_{,z}[r]\,\mathbf{u}_{,y}[c]\,C_{55}\,F_\tau\,F_{s_{,z}}\,N_{i_{,y}}\,N_j > \\
+\;& < P_{21}P_{31}\mathbf{u}_{,z}[r]\,\mathbf{u}_{,y}[c]\,C_{23}\,F_{\tau_{,z}}\,F_s\,N_i\,N_{j_{,y}} > + < P_{41}P_{51}\mathbf{u}_{,z}[r]\,\mathbf{u}_{,y}[c]\,C_{45}\,F_\tau\,F_{s_{,z}}\,N_{i_{,x}}\,N_j > \\
+\;& < P_{31}P_{61}\mathbf{u}_{,z}[r]\,\mathbf{u}_{,y}[c]\,C_{36}\,F_{\tau_{,z}}\,F_s\,N_i\,N_{j_{,x}} >
\end{aligned}
$$

In the formulations given above, $\mathbf{u}_{,x}[r]$ denotes the r-th component of the vector $\partial\mathbf{u}/\partial x$ (e.g. $\mathbf{u}_{,x}[2] = u_{y,x}$). Analogously, $\mathbf{u}_{,y}[c]$ represents the c-th component of the vector $\partial\mathbf{u}/\partial y$, etc.

References

[1] M. Amabili. *Nonlinear Mechanics of Shells and Plates in Composite, Soft and Biological Materials*. Cambridge University Press, New York, USA, 2018.

[2] A. H. Nayfeh and P. F. Pai. *Linear and nonlinear structural mechanics*. John Wiley & Sons, 2008.

[3] J. N. Reddy. *An Introduction to Nonlinear Finite Element Analysis: with applications to heat transfer, fluid mechanics, and solid mechanics*. Oxford University Press, Oxford, 2014.

[4] S. Levy, D. Goldenberg, and G. Zibritosky. Simply supported long rectangular plate under combined axial load and normal pressure. *National Advisory Committee for Aeronautics, Technical Note*, No. 949, 1944.

[5] A. G. Striz, S. K. Jang, and C. W. Bert. Nonlinear bending analysis of thin circular plates by differential quadrature. *Thin-Walled Structures*, 6(1):51–62, 1988.

[6] E. Carrera and M. Villani. Large deflections and stability FEM analysis of shear deformable compressed anisotropic flat panels. *Composite Structures*, 29(4):433–444, 1994.

[7] D. W. Murray and E. L. Wilson. Finite-element large deflection analysis of plates. *Journal of the Engineering Mechanics Division*, 95(1):143–166, 1969.

[8] S. Levy. Bending of rectangular plates with large deflections. *NACA Technical Note*, No. 737, 1942.

[9] S. Levy. Square plate with clamped edges under normal pressure producing large deflections. *NACA Technical Note*, No. 740, 1942.

[10] K. R. Rushton. Large deflection of variable-thickness plates. *International Journal of Mechanical Sciences*, 10(9):723–735, 1968.

[11] G. J. Turvey and M. Y. Osman. Elastic large deflection analysis of isotropic rectangular Mindlin plates. *International Journal of Mechanical Sciences*, 32(4):315–328, 1990.

[12] Farbod Alijani and Marco Amabili. Non-linear static bending and forced vibrations of rectangular plates retaining non-linearities in rotations and thickness deformation. *International Journal of Non-linear Mechanics*, 67:394–404, 2014.

[13] Farbod Alijani and Marco Amabili. Effect of thickness deformation on large-amplitude vibrations of functionally graded rectangular plates. *Composite Structures*, 113:89–107, 2014.

[14] B Wu, A Pagani, M Filippi, WQ Chen, and E Carrera. Large-deflection and post-buckling analyses of isotropic rectangular plates by carrera unified formulation. *International Journal of Non-Linear Mechanics*, 2019.

[15] J. N. Reddy and W. C. Chao. Non-linear bending of thick rectangular, laminated composite plates. *International Journal of Non-Linear Mechanics*, 16(3-4):291–301, 1981.

[16] C. Y. Chia. Large deflection of unsymmetric laminates with mixed boundary conditions. *International Journal of Non-Linear Mechanics*, 20(4):273–282, 1985.

[17] Y. Urthaler and J. N. Reddy. A mixed finite element for the nonlinear bending analysis of laminated composite plates based on FSDT. *Mechanics of Advanced Materials and Structures*, 15(5):335–354, 2008.

[18] K. K. Shukla and Y. Nath. Nonlinear analysis of moderately thick laminated rectangular plates. *Journal of Engineering Mechanics*, 126(8):831–838, 2000.

[19] P. Dash and B. N. Singh. Geometrically nonlinear bending analysis of laminated composite plate. *Communications in Nonlinear Science and Numerical Simulation*, 15(10):3170–3181, 2010.

[20] E. Carrera and B. Kröplin. Zigzag and interlaminar equilibria effects in large-deflection and postbuckling analysis of multilayered plates. *Mechanics of Composite Materials and Structures*, 4(1):69–94, 1997.

[21] H. B. Coda. Continuous inter-laminar stresses for regular and inverse geometrically nonlinear dynamic and static analyses of laminated plates and shells. *Composite Structures*, 132:406–422, 2015.

[22] H. B. Coda, R. R. Paccola, and R. Carrazedo. Zig-zag effect without degrees of freedom in linear and nonlinear analysis of laminated plates and shells. *Composite Structures*, 161:32–50, 2017.

[23] A. W. Leissa. Buckling of laminated composite plates and shell panels. *Flight Dynamics Laboratory Report*, AFWAL-TR-85-3069, 1985.

[24] L Librescu and M. Y. Chang. Imperfection sensitivity and postbuckling behavior of shear-deformable composite doubly-curved shallow panels. *International Journal of Solids and Structures*, 29(9):1065–1083, 1992.

[25] G. J. Turvey and I. H. Marshall. *Buckling and postbuckling of composite plates*. Springer Science & Business Media Dordrecht, 1995.

[26] A. Pagani and E. Carrera. Unified formulation of geometrically nonlinear refined beam theories. *Mechanics of Advanced Materials and Structures*, 25(1):15–31, 2018.

[27] A. Pagani and E. Carrera. Large-deflection and post-buckling analyses of laminated composite beams by Carrera Unified Formulation. *Composite Structures*, 170:40–52, 2017.

[28] A. Pagani, E. Carrera, and R. Augello. Evaluation of various geometrically nonlinear terms in the static response of beams and thin-walled shell-like structures. *Submitted*, 2019.

[29] T. von Kármán. Festigkeitsprobleme in maschinenbau. *Enzyklopaedie der Mathematischen Wissenschaften*, 4:311–385, 1910.

[30] E. Carrera, M. Cinefra, M. Petrolo, and E. Zappino. *Finite Element Analysis of Structures through Unified Formulation*. John Wiley & Sons, Chichester, West Sussex, UK, 2014.

[31] E. Carrera, A. Pagani, and M. Petrolo. Classical, refined and component-wise theories for static analysis of reinforced-shell wing structures. *AIAA Journal*, 51(5):1255–1268, 2013.

[32] E. Carrera and A. Pagani. Accurate response of wing structures to free vibration, load factors and non-structural masses. *AIAA Journal*, 54(1):227–241, 2016.

[33] E. Carrera, A. Pagani, and M. Petrolo. Refined 1D finite elements for the analysis of secondary, primary, and complete civil engineering structures. *Journal of Structural Engineering*, 141:04014123/1–14, 2015.

[34] E. Carrera and A. Pagani. Free vibration analysis of civil engineering structures by component-wise models. *Journal of Sound and Vibration*, 333(19):4597–4620, 2014.

[35] K. J. Bathe. *Finite Element Procedure*. Prentice Hall, Upper Saddle River, New Jersey, USA, 1996.

[36] B. Wu, A. Pagani, M. Filippi, W. Q. Chen, and E. Carrera. Accurate stress fields of post-buckled laminated composite beams accounting for various kinematics. *International Journal of Non-Linear Mechanics*, 111:60–71, 2019.

[37] M. A. Crisfield. A fast incremental/iterative solution procedure that handles "snap-through". *Computers & Structures*, 13(1):55–62, 1981.

[38] M. A. Crisfield. An arc-length method including line searches and accelerations. *International Journal for Numerical Methods in Engineering*, 19(9):1269–1289, 1983.

[39] E. Carrera. A study on arc-length-type methods and their operation failures illustrated by a simple model. *Computers & Structures*, 50(2):217–229, 1994.